Clean Energy Science and Technology 2024, 2(2), 134
https://doi.org/10.18686/cest.v2i2.134

Article

Polymeric field synergy principle: Revealing the intrinsic mechanism of screw channel optimization to enhance thermal management and process efficiency

Wei Pan[1], Shizheng Huang[1], Jiawei Zhu[1], Xiankui Zeng[1], Weimin Yang[2], Ranran Jian[1,*]

[1] College of Electromechanical Engineering, Qingdao University of Science and Technology, Qingdao 266061, Shandong Province, China
[2] College of Mechanical and Electrical Engineering, Beijing University of Chemical Technology, Beijing 100029, China
*** Corresponding author:** Ranran Jian, jianrr@qust.edu.cn

CITATION

Pan W, Huang S, Zhu J, et al. Polymeric field synergy principle: Revealing the intrinsic mechanism of screw channel optimization to enhance thermal management and process efficiency. Clean Energy Science and Technology. 2024; 2(2): 134. https://doi.org/10.18686/cest.v2i2.134

ARTICLE INFO

Received: 29 February 2024
Accepted: 7 April 2024
Available online: 10 April 2024

Abstract: The process efficiency and energy efficiency of extrusion equipment emerge as pivotal challenges constraining the development of the polymer extrusion industry. This article presents a new principle of polymeric field synergy to guide the solution to the low mixing efficiency and energy utilization efficiency of traditional extrusion equipment. Finite element analysis was conducted on four novel unconventional screw configurations and compared with the traditional single-thread screw. Results revealed that more complicated melt flow patterns generated in the modified novel screw configurations enhanced the stretching deformation or helical flow. The stretching or helical flows to varying degrees during the melt extrusion process thereby improved the mixing and heat transport efficiency. Among them, helical flow induced by the Maddock element exhibited the most significant impact on stretching flow and ductile deformation in the flow field. Simultaneously, the helical flow caused radial motion of the internal material, significantly promoting the synergy between the velocity field, velocity gradient field, and temperature gradient field. This enhanced radial heat and mass transport efficiency within the screw channel, subsequently improving the overall operational efficiency of the equipment. The results of the finite element analysis have substantiated the scientific validity of the polymeric field synergy principle.

Keywords: polymer extrusion; mixing efficiency; heat and mass transport efficiency; energy utilization efficiency; field synergy principle

1. Introduction

With the worsening of the energy crisis and environmental problems, the goals for peaking carbon emissions and achieving carbon neutrality have been brought to a national strategy by many countries [1,2]. Thus, developing low-energy, high-efficiency green processing and forming technologies and equipment has become a development trend in the polymer mechanical industry [3,4].

In polymer extrusion processing, the efficiency of mixing processes and energy utilization has consistently been a focal point of research. In traditional screw extrusion system, the flow field is advection-dominated because of the high viscosity of the melt, and the heat transfer process is limited in general owing to the low thermal conductivity of polymers, which results in uneven temperature and heat distribution, inefficient plasticization, and high energy consumption, etc. The operational mode of traditional extrusion equipment exhibits a low energy utilization rate, earning it the designation of “high-energy consuming” equipment within the mechanical industry [5,6]. Improving the thermal management and process efficiency of the extrusion

system is particularly crucial. To enhance the efficiency of extrusion equipment, a variety of novel extrusion screws have been developed, such as Maillefer-type barrier screw, pin screw, wavy screw, and Maddock screw, etc.

In general, a homogenous melt distribution and heat management can be achieved by increasable mixing with shear heating. For instance, Dray [7] simulated the melting capability of various barrier mixing screws and developed a computer model to character the melting capabilities of screws with different barrier designs. Results indicated that Maillefer-type barrier screw configuration achieved additional melting area by eliminating solids-bed breakup compared to the non-barrier screw. This increased the melting capacity from 482 lb/hr to 539 lb/hr. Chen et al. [8] investigated the flow field in the mixing section of a pin-barrel single-screw extruder compared with a conventional single-screw one, evaluating the mixing performance of these two mixing approaches. Results indicated that the introduction of pins can disrupt the particle flow trajectories and alter the particle movement direction, facilitating an increase in stretching rates and thereby enhancing the mixing efficiency. Liu et al. [9] conducted a numerical simulation study on the mixing performance of wavy screw elements and barrier screw elements using the CFD software ANSYS POLYFLOW. Results demonstrated that the periodic depth variations of the wavy screw elements can enhance shear and stretching effects, resulting in improved mixing, higher efficiency, and more uniform thermal distribution. Spalding et al. [10] provided guideline for obtaining optimal mixing stress by describing the mechanisms occurring in the Maddock mixer. Results indicated that extrusion via the Maddock mixer can eliminate compositional and thermal gradients within the extrudates, demonstrating excellent performance in reducing solid polymer fragments and unmixed gels in the extrudates.

Besides, enhancing the heat transport process during extrusion can facilitate the thermal management and energy efficiency. Considering the fact that heat transfer is mainly influenced by the ductile flow state, controlling the flow pattern is an effective way to enhance heat transfer, which is highly related with the screw structures. Formela et al. [11] used a co-rotating twin screw extruder with a specially configured plasticizing unit to continuously recover ground tire rubber (GTR). The results of thermogravimetric analysis indicated that the thermal stability of regenerated GTR largely depends on the screw structure. Jian et al. [12] proposed a novel “flipping melt-pancakes” screw structure by designing torsional flow pattern to enhance molecular and thermal mobility between the top area and the bottom area in the radial of screw channel, and results indicated that effective transfer of local heat occurred to achieve uniform thermal distribution. Afterwards, Jian et al. [13] proposed yet another novel “stretching melt-pancakes” screw structure to generate elongational flow and compared it with traditional screw and “flipping melt-pancakes” structures. The elongation deformation caused by the converging wedge-shaped channel of the “stretching melt-pancakes” screw structure can enhance radial mass and heat transfer, achieving effective mixing of local heat and particles. Researches mentioned above has shown that controlling the flow pattern though design and optimization of screw structure is an effective method.

While the above-mentioned study has confirmed the excellent performance of the novel screw configurations in the industrial domain, in depth analysis of underlying mechanisms remain to be addressed. The melt flow in the polymer extrusion process is highly intricate, involving various viscoelastic flow forms such as stretching flow and shear flow [14], brought with viscous dissipation, rheological properties, etc. The impact mechanisms of these screws on flow and thermal transport lack effective theory for a unified explanation.

In this paper, a theoretical analysis of extrusion process was carried out, delving into the interrelationships among velocity field, velocity gradient field, and temperature gradient field [15], and the polymeric field synergy principle was proposed to elucidate the intrinsic mechanisms of heat and mass transport in the molten polymer during the extrusion process [16]. In order to validate the scientific validity of the proposed theory, four representative unconventional novel screws, widely used in industry, were selected to analyze and compared them with a standard screw.

2. Polymeric field synergy principle

To overcome the challenge of weak thermal and mass transport capacity during polymer melt extrusion plasticization and improve the energy utilization efficiency, we proposed a new and widely applicable polymeric field synergy principle. Based on the analysis of polymer processing rheology and fluid mechanics, the core idea of polymeric field synergy principle is elaborated in detail, which is divided into mixing synergy and heat transfer synergy [17].

2.1. Mixing synergy

The momentum conservation Equation (1) during polymer extrusion process is as follows.

$$\rho \frac{D\vec{v}}{Dt} = \nabla \cdot \vec{\tau} - \nabla P + \rho g \tag{1}$$

The left-hand side of Equation (1) represents the fluctuation in fluid momentum, characterized by its association with two vectors-velocity and velocity gradient. These vectors serve to indicate, to a certain degree, the intensity of mass transfer and mixing during polymer extrusion. The terms on the right-hand side comprise viscous stress, static pressure, and gravitational components, respectively. Through further expansion, we can get Equation (2).

$$\rho(\frac{\partial \vec{v}}{\partial t} + \vec{v} \cdot \overrightarrow{\nabla v}) = \nabla \cdot \vec{\tau} - \nabla P + \rho g \tag{2}$$

where ρ, v, t, τ, P and g are the density, velocity, time, stress, pressure, and gravitational acceleration, respectively. Equation (2) reveals a scalar product between velocity and velocity gradient, affecting the alteration in momentum increment across the entire fluid domain. This dot product can be expanded into Equation (3).

$$\vec{v} \times \overrightarrow{\nabla v} = \left|\vec{v}\right| \times \left|\overrightarrow{\nabla v}\right| cosa \tag{3}$$

Equations (2) and (3) imply that the momentum increment and mass transfer are contingent not only upon the magnitudes of velocity and velocity gradient but also on

their intersection angle. In other words, the interaction relationship between velocity and velocity gradient—the intersection angle—is one of the key factors that affects the momentum of the fluid domain. As the intersection angle α approaches zero, the dot product attains its maximum, exerting the most substantial impact on momentum increment. Conversely, when the intersection angle α reaches 90°, the dot product becomes zero, resulting in minimal effects on momentum increment. Accordingly, the intersection angle should be as small as possible to maximize the interconnection of velocity and velocity gradient. This also explain the fact that the stretch flow mixing is better than shear flow. As shown in **Figure 1(a)** and **1(b)**, in a pure shear flow field, the angle between velocity and velocity gradient reaches 90°, while in a pure elongational flow field, the intersection angle converges to 0°.

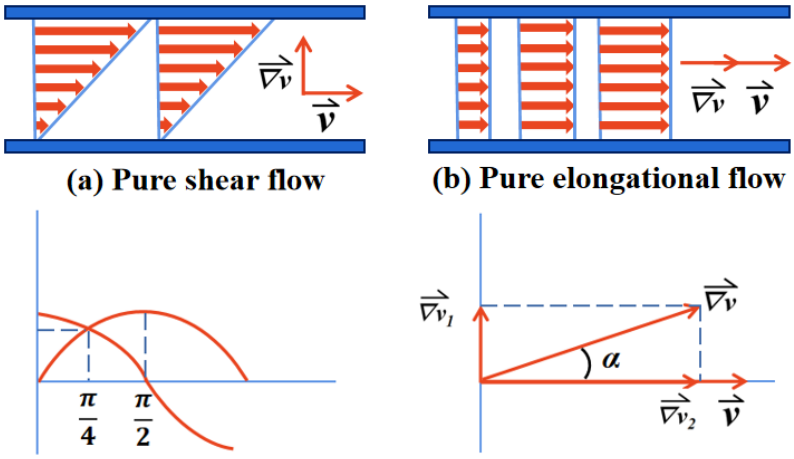

Figure 1. Basic ductile deformation and its vector relation.

The synergistic equations of the mixing-enhanced field in the flow process of polymer melt, derived through the conservation of momentum, can be employed to analyze the synergy between the velocity field and velocity gradient field, and their relationship with shear flow and stretching flow. In **Figure 1(c)**, it can be seen that the smaller the angle α between velocity and velocity gradient, the higher the proportion of extensional flow, and the greater the momentum increment. Fundamentally, the impact of extensional flow on mixing stems from the maximization of momentum increment. This allows a novel possibility to understand the physical issues in polymer processing from the perspective of field synergy. To enhance mixing, it is preferable to employ ductile deformation, such as squeezing or stretching, not just relying on shear.

2.2. Heat transfer synergy

The energy conservation in the polymer processing can be expressed by Equation (4).

$$\rho C_V \frac{DT}{Dt} = -\nabla \cdot \vec{q} - T\left(\frac{\partial P}{\partial T}\right)_P (\nabla \cdot \vec{v}) + (\vec{\tau} : \nabla \cdot \vec{v}) \tag{4}$$

The left-hand term in Equation (4) corresponds to the increase in internal energy, signifying alterations in heat. The three terms on the right side encompass heat transfer energy, energy variations due to fluid expansion or compression per unit volume, and viscous dissipation energy, respectively. The second term on the right side of Equation (4) is negligible for incompressible polymers. Upon additional expansion, Equation (5) is derived as follows.

$$\rho C_V(\frac{\partial T}{\partial t}+\vec{v}\cdot\overrightarrow{\nabla T})=-\nabla\cdot(-K\overrightarrow{\nabla T})+(\vec{\tau}:\nabla\cdot\vec{v}) \tag{5}$$

where C_V, T and K are the constant-volume specific heat, temperature and heat transfer coefficient, respectively. From Equation (5), we can find a scalar product of velocity and temperature gradient, which affects the change of internal energy in the whole fluid domain. This dot product can be expanded into Equation (6).

$$\vec{v}\cdot\overrightarrow{\nabla T}=\left|\vec{v}\right|\times\left|\overrightarrow{\nabla T}\right|cos\beta \tag{6}$$

Likewise, it can be inferred that internal energy and heat transfer rely not only on the magnitudes of velocity and temperature gradient but also on their intersection angle. A small intersection angle β leads to a large heat transfer coefficient K under a constant viscous dissipation power. This provides a novel approach for enhancing heat transfer in polymer processing.

The schematic in **Figure 2** visually illustrates this synergistic effect. When the flow direction of unheated molecules has a component towards to the heated ones, i.e., the flow direction between them is not perpendicular, they expect to have more probability to coalesce with each other and exchange heat, thereby, achieving a more uniform heat distribution.

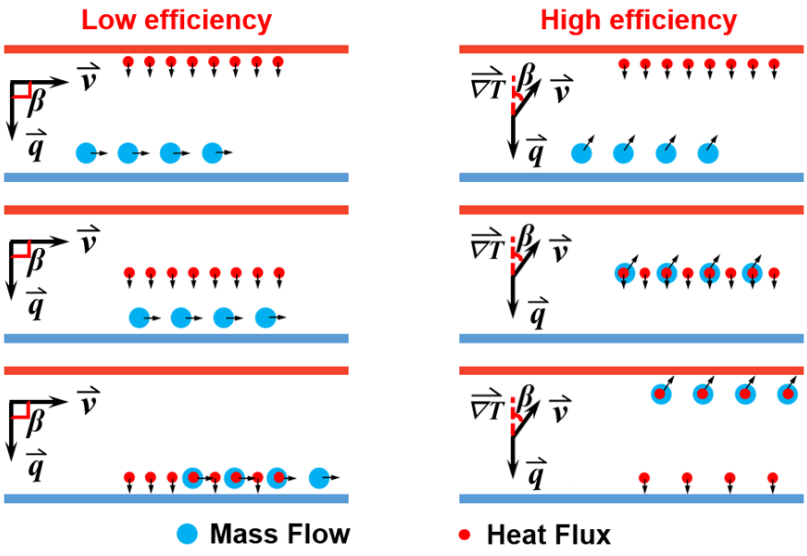

Figure 2. Schematic of the synergy between flow and thermal transport.

3. Model and method

3.1. Physical model

The geometric structures of the five studied screws are illustrated in **Figure 3**. Among them, **Figure 3(a)** displays a standard single-threaded screw (STD) in

industry, which is used for the purpose of comparison in this work. **Figure 3(b)** was the Maillefer-type barrier (BM) screw, which adds an auxiliary thread in the single-threaded screw to separate the solid and melt in the screw groove. **Figure 3(c)** shows a Pin screw that has 5 rows of neatly arranged pins placed at the head of a single-threaded screw, which is the most common screw structure in the diffluent-type screw. **Figure 3(d)** and **3(e)** represent the wavy screw and Maddock screw, respectively, widely utilized as typical examples of the variable-channel screw and barrier screw. Among them, the wavy screw adopts a wavy single screw element with an eccentricity of 3mm, and the Maddock element has 8 deep channels and 4 shallow channels.

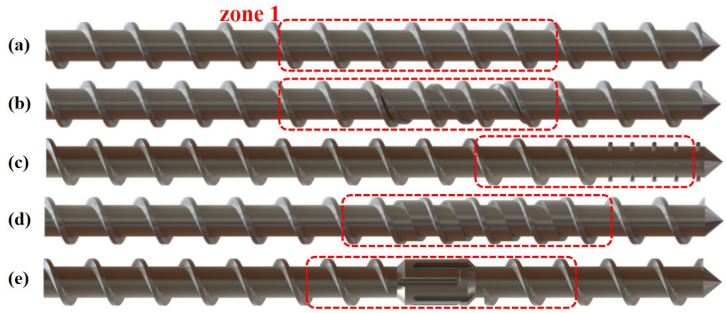

Figure 3. The studied screw: **(a)** Single-thread screw; **(b)** BM screw; **(c)** Pin screw; **(d)** Wavy screw; **(e)** Maddock screw.

The region between the barrel wall and screw surface constituted the flow domain. To avoid the influence of the inlet, the flow domain was extended by 2 mm from the inlet of screw. The specific model is depicted in **Figure 4**, with the geometric parameters detailed in **Table 1**.

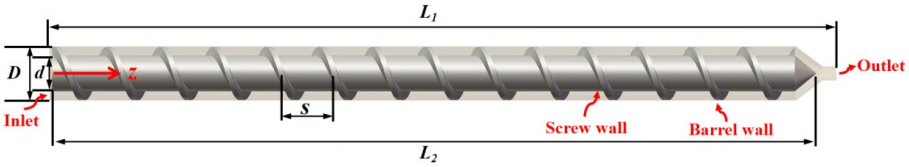

Figure 4. Single-thread screw and working fluid model.

Table 1. Geometric parameters of the physical model.

Parameter	Symbol	Value/mm
Barrel length	L_1	445
Screw length	L_2	432
Screw diameter	D	30
Screw root diameter	d	20
Screw pitch	S	30

3.2. Governing equations and boundary conditions

The extrusion process of high-viscosity polymers is highly complex, involving passive flow, viscous dissipation, ductile deformation, and heat and mass transfer, etc. The simulated flow medium employed in this study was ethylene propylene diene monomer (EPDM). It was assumed that the melt behaved as an incompressible viscous

non-Newtonian fluid, and the flow exhibited a laminar non-isothermal transient behavior. The melt fully occupies the entire flow channel, and there is no slip on the wall. Given that EPDM is a high viscoelastic rubber, its flow is predominantly governed by viscous force, thus the inertial force was negligible. With the above assumptions, the working flow field followed three governing equations of fluid mechanics—mass, momentum, and energy conservation equations, respectively—as follows [18].

Mass conservation equation,

$$\frac{\partial u_i}{\partial x_i} = 0 \tag{7}$$

Momentum conservation equation,

$$\rho \frac{\partial u_i}{\partial t} + \frac{\partial P}{\partial x_i} = \frac{\partial}{\partial x_j}(\eta \frac{\partial u_i}{\partial x_j}) \tag{8}$$

Energy conservation equation,

$$\rho C_P (\frac{\partial T}{\partial t} + u_i \frac{\partial T}{\partial x_i}) = k \frac{\partial^2 T}{\partial x_i^2} + \varphi \tag{9}$$

The constitutive equation is used describe the rheological properties of EPDM using the Bird-Carreau law and approximate Arrhenius law [19],

$$\eta = [\eta_\infty + (\eta_0 - \eta_\infty)(1 + \lambda^2 \dot{\gamma}^2)^{\frac{n-1}{2}}] exp[-f(T - T_\alpha)] \tag{10}$$

The pertinent characteristics of EPDM employed in the simulation were provided in **Table 2**, whereas the boundary conditions can be found in **Table 3**.

Table 2. Properties of EPDM used in the simulation.

Parameter	Symbol	Value
Density	ρ	1150 Kg/m^3
Specific heat capacity	C_p	1600 J/(Kg·K)
Thermal conductivity	k	0.25 W/(m·K)
Viscosity at an infinite shear rate	η_∞	0 Pa·s
Zero shear viscosity	η_0	175000 Pa·s
Natural time	λ	14 s
Non-Newtonian index	n	0.408
Coefficient of temperature sensibility	f	0.0025 K^{-1}
Reference temperature	T_α	373.15 K

Table 3. Boundary conditions.

Boundary	Flow conditions	Thermal conditions
Inlet	Fully developed, volumetric flow rate 2.44 × 10^{-6} m^3/s	353.15 K (80 °C)
Outlet	Flow outflow	Heat outflow
Barrel wall	Stationary, no-slip wall	343.15 K (70 °C)
Screw wall	Screw speed 60 r/min	Insulated boundary

3.3. Mesh system and independence validation

In this work, the computational fluid dynamics (CFD) software of ANSYS Polyflow 2021 R1 (ANSYS, Inc., USA) was used for the calculation and the mesh systems were generated by ANSYS Mesh 2021 R1 meshing software (ANSYS, Inc., USA). The fluid domain was discretized using a hexahedral structural grid, with the boundary layer mesh near the barrel being refined to ensure computational accuracy. Due to the irregular structures of the screw models, the screw parts were discretized using tetrahedral non-structural grid. Finally, mesh superposition technique was employed to generate an integrated finite element mesh for both the fluid domain and the screw moving part.

To ensure the reliability of the simulation results, an independent validation of the fluid grid model was conducted. **Figure 5** illustrates the variation of the average velocity and average temperature of the melt with different fluid grid at a rotational speed of 60 r/min. The evaluation of grid was performed in the radial (R), circumferential (C) and axial (L) dimensions. Considering a balance between computational efficiency and accuracy, the grid configuration of 18 × 70 × 180 layers will be adopted in the subsequent numerical simulations, with a total grid count of 263,563.

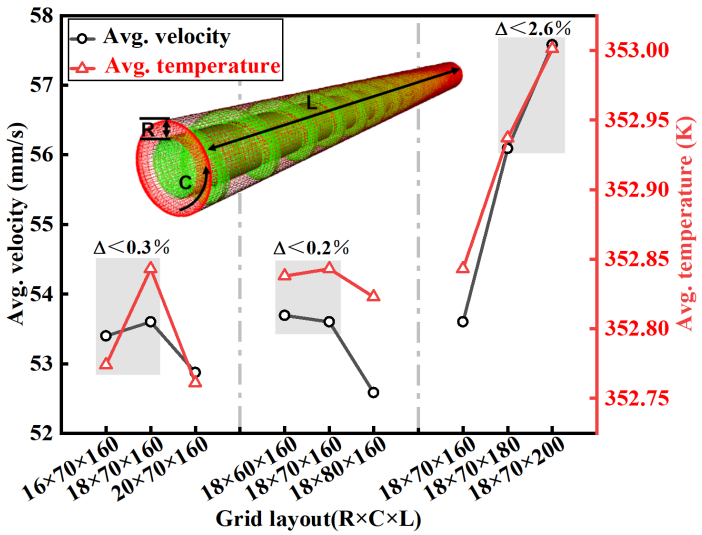

Figure 5. Mesh independence validation of fluid model.

4. Result and discussion

4.1. Analysis of melt flow patterns

The structure of the screw determines the flow characteristics of the polymer melt, subsequently influencing both mixing and heat transfer performance. To clearly illustrate the distinct flow patterns of different screws, we adopted rotating reference frame with the barrel rotation reversely around the static screw. The flow pattern at zone 1 position of five screws can be found in **Figure 6**. From **Figure 6(a)**, it is evident that in the STD screw, the melt is transported forward in the form of plunger advection-flow along the channels of the screw elements with little radial motion. In the BM screw, most particles first accumulated in the narrow channel formed by the auxiliary

thread and the preceding main thread (i.e., solids-bed area), and crossed over the auxiliary thread to the main channel after melting, achieving good separation of melt and solids-bed. This phenomenon has also been acknowledged in Gaspar-Cunha's work [20]. The streamline trajectories of the pin screw revealed a distinct diversion phenomenon occurring at the pin location. The eccentric structure of the wavy screw leaded to a periodic variation in the radial channel depth. The flow tended to shift towards the deeper regions, resulting in extensional flow in the variational cross section. The unique structural design of the Maddock element with alternating deep and shallow channels, interacting with the inner wall of the barrel, induced radial rolling of the particles in the deep channels, resulting in a distinctive helical flow pattern. In the cross-sectional streamlines shown in **Figure 6(b)**, the vortex exhibited in the deep channels of Maddock element also provide good evidence of this. Besides, almost no radial flow occurred among these screws except the Maddock element and the intersection of deep and shallow channels of wavy screw.

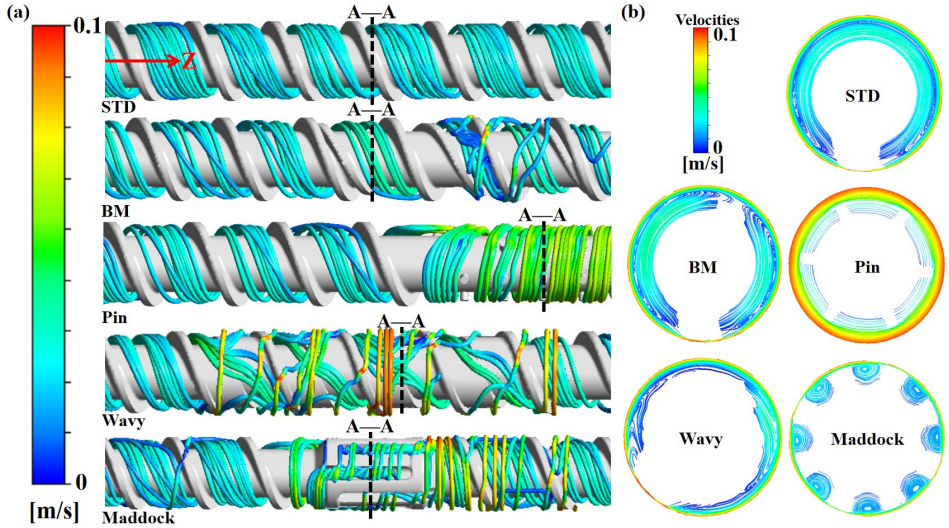

Figure 6. (a) Melt flow patterns in the rotating reference frame: velocity streamline in the axial direction; **(b)** the axial velocity in the cross-section A-A.

4.2. Mixing performance and synergistic analysis

The efficiency of mixing process is a crucial factor in evaluating the performance of extrusion equipment. **Figure 7** presents a series of commonly used indicators to assess the efficiency of mixing process. Among them, the segregation scale reflects the uniformity of concentration field in the mixing phases to characterize mixing capability. A smaller segregation scale indicates a more uniform mixing. As shown in **Figure 7(a)**, among the five types of screws, the STD screw exhibited the highest segregation scale, while the segregation scale values for all of the four modified novel screws decreased, with the Maddock screw being the lowest, next is the wavy screw. This indicated that the STD screw has the lowest level of mixing uniformity, resulting in the poorest mixing. The other four novel screw designs, to some extent, improved the uniformity of mixing, especially the Maddock screw.

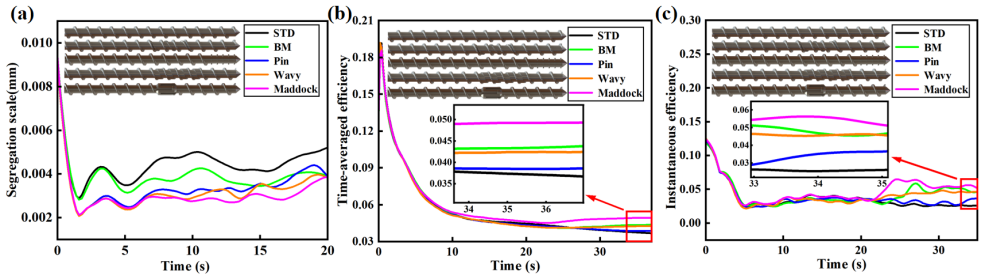

Figure 7. (a) Mixing performance evaluation: segregation scale; **(b)** time-averaged mixing efficiency; **(c)** instantaneous mixing efficiency.

The mixing efficiency characterizes the extent of area extension induced by the stretching action and quantifies the ability of flow deformation to reflect distribution mixing. A higher mixing efficiency indicates better mixing capability. **Figures 7(b)** and **7(c)** illustrate the time-averaged and the instantaneous mixing efficiency curves over time for the five screws. It can be observed that the time-averaged mixing efficiency was highest for the Maddock screw, followed by the BM screw and the wavy screw, while the STD screw exhibited the lowest. The results indicated that, compared to the other four screw types, the helical flow generated by the Maddock element can significantly enhance deformation in the melt flow, leading to a substantial increase in the mixing efficiency. The order of instantaneous mixing efficiency for the five screw types in **Figure 7(c)** is: Maddock > BM ≈ Wavy > Pin > STD, consistent with the trends depicted in **Figure 7(b)**. Additionally, combined with Zitzenbacher's work [21], it can be clearly indicated that the Maddock element exhibited well in enhancing screw mixing.

To further explore the intrinsic mechanisms of the mixing enhancement by the Maddock element, flow field analysis was performed on both the STD and Maddock screws. **Figure 8** presents the axial cross-sectional streamline trajectory cloud maps. It was found that the fluid only underwent simple shear laminar flow in STD channels, with almost no change in the velocity magnitude in each radial layer. The direction of velocity gradient was almost parallel to the radial direction of the screw groove, while there was a significant change in velocity in Maddock channels, and velocity gradient was no longer parallel to the radial direction of the screw groove. It can be concluded that the helical flow induced by the Maddock element enhanced the radial mass transfer, brought good synergy between velocity and velocity gradient, resulting in improvement in the mixing process during the extrusion process.

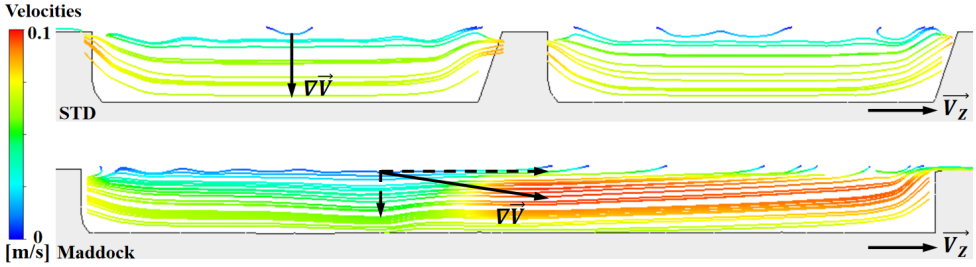

Figure 8. Axial velocity streamlines with the screw channels for STD and Maddock.

To further validate the mixing enhancement mechanism of the four unconventional screw configurations, field synergistic analysis was carried out on these five screws, including the STD screw. **Figure 9(a)** illustrates the distribution of the synergy angle α between the axial velocity and axial velocity gradient along the axial position for the five screws. It is evident that, compared to the STD screw, the synergy angle α values decreased at the element locations of the unconventional screw. Among them, Maddock element had the lowest synergy angle α, Pins being second. According to the polymeric field synergy principle, it can be inferred that the decrease in the synergy angle α is attributed to the occurrence of extensional flow at the element locations, which was further validated in **Figure 9(c)**.

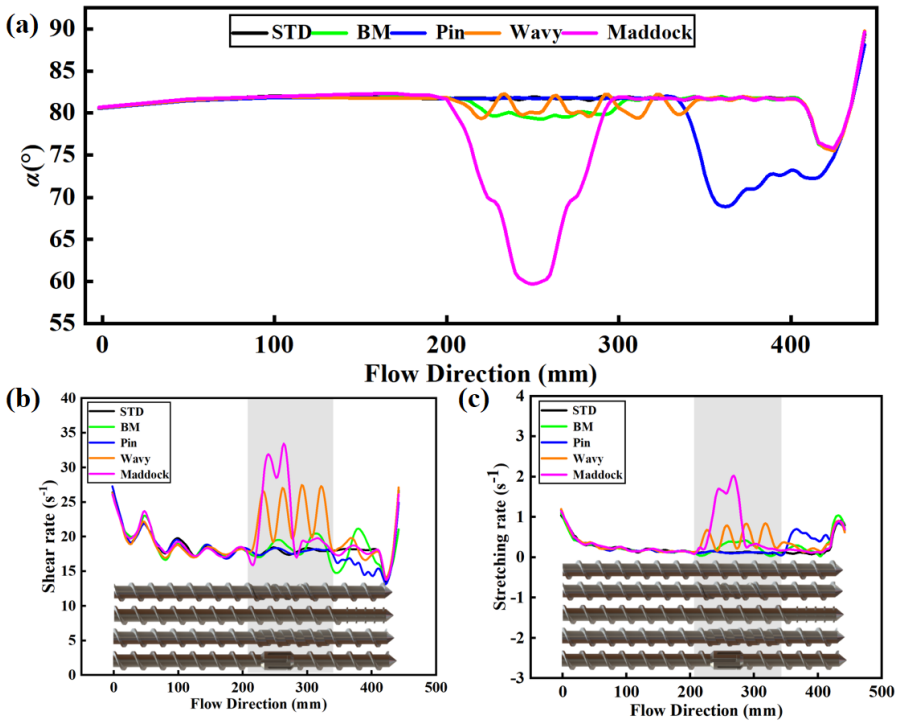

Figure 9. Mixing synergy and ductile deformation for screws: **(a)** synergy angle α along the flow direction; **(b)** shear rate distribution and **(c)** stretching rate distribution.

In **Figure 9(b)**, it can be seen that the order of shear rate of the different screws was: Maddock > Wavy > BM > STD > Pin. In **Figure 9(c)**, it can be observed that the stretching rate is highest at the Maddock, followed by Wavy, Pin, BM, and STD in sequence. Resulted indicated that the unconventional screw structure enhanced both the shear and stretching deformation. In the BM screw, as particles entered the continuously narrow channel and passed over the auxiliary thread, it was subjected to shear and stretching effects. The pins of the pin screw can force the diversion of the fluid, generate stretching flow, and enhance the stretching rate, but the shear action was weakened, which is consistent with Chen et al.'s work [8]. The wavy screw caused periodic strong shear and stretching effects as the flow passed through the screw channels with the periodic variation in the depth because of its eccentric structure. In Dörner et al.'s work [22], this regular change is considered the fundamental reason for improving the mixing performance of the wavy screw. Besides, the Maddock screw

performed strong shear and stretching simultaneously. The shallow channels brought powerful shear forces on the melt, while the variations in channel depth and helical flow generated in the deep channels significantly increased the stretching flow and deformation. Accordingly, the mixing capacities improved of the unconventional screws. Despite all this, the flow field was still shear-dominated for all these five screws because the synergy angle α values were higher than 45°.

4.3. Thermal performance and synergistic analysis

In the extrusion process of polymer plasticization, the efficiency of heat transfer in the melt is relatively limited owing to the extremely low thermal diffusivity, generally, leading to high radial temperature difference. The radial temperature distribution of five distinct screw types was investigated, and the findings are illustrated in **Figure 10**.

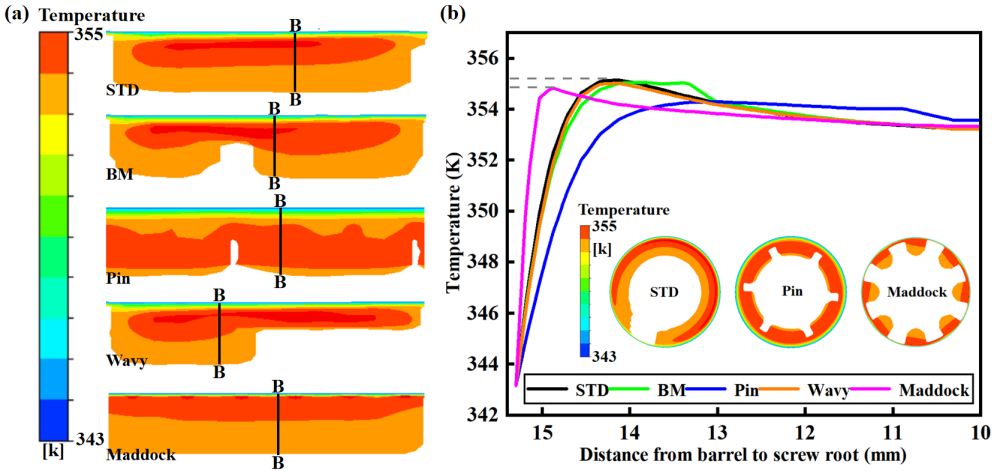

Figure 10. Heat transfer performance: **(a)** temperature fields for various screw elements; **(b)** radial distribution of temperature at section B-B.

Figure 10(a) shows the temperature fields of five types of screws. It can be observed that the high-temperature region at the Maddock element was closer to the barrel. This is due to the helical flow induced by the Maddock element, realizing the mass and heat exchange from the bottom to the top of channel, leading to the upward extension of the high-temperature region. However, the pin screw showed the poorest heat transfer, even worse than the STD screw. **Figure 10(b)** illustrates the radial temperature distribution at the cross-section B-B. It was found that, compared to the STD screw, other four screws exhibited a reduction in the maximum temperature. Among them, the temperature of the Pin element was lowest, followed by the Maddock element. A possible explanation is because of the weak shear ability of the Pin element. This did not necessarily indicate that the heat transfer ability of the Pin element is good, as further evidenced by the convective heat transfer coefficient in **Figure 11(a)**. Unlike the Pin element, the Maddock element was due to its ability to generate helical flow that promoted the heat and mass transport in the melt, greatly enhancing heat transfer capability. Additionally, the radial temperature distribution curve of the Maddock element trended to left, again revealing the extension of the

high-temperature region towards the inner wall of the barrel. This, to a certain extent, facilitated the cooling effect the barrel.

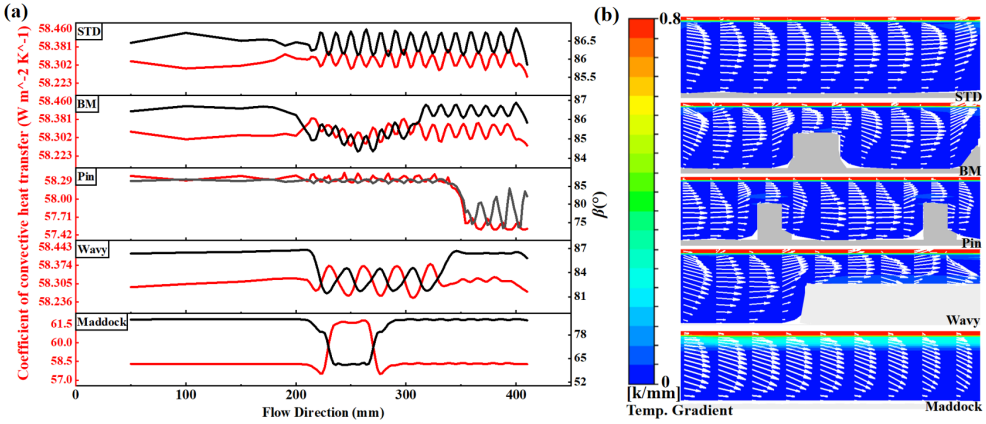

Figure 11. (a) Heat transfer performance along the flow direction; **(b)** the temperature gradient contours and axial velocity vector with the screw channels for screws.

The magnitude of the convective heat transfer coefficient reflects the intensity of convective heat transfer. **Figure 11(a)** depicts the distribution of convective heat transfer coefficients along the axial positions of the five screws, as well as the synergy angle β between velocity and temperature gradient. The convective heat transfer coefficient of the unconventional screws improved except the pin screw. The synergy angle β values for Maddock element was the smallest, and the convective heat transfer coefficient was the largest. This indicated that the Maddock screw element exhibited the best heat transfer performance. Furthermore, it is evident in **Figure 11(a)** that there was negative correlation between the convective heat transfer coefficient and the synergy angle β, which agrees very well with the polymeric field synergy principle. The axial velocity vector and temperature gradient contour maps were illustrated in **Figure 11(b)**. Results showed that the velocity vectors are nearly parallel to the isotherms for STD screw, indicating that there was almost no synergy between velocity field and temperature gradient field. In the unconventional screws, velocity had a radial offset at specific locations, such as near the auxiliary thread of BM screw, near the pins of pin screw, and the transition of screw channel depth of wavy screw, thereby enhancing the synergistic interaction between velocity field and temperature gradient field. In particular, the helical flow in Maddock element caused the velocity to radial offset throughout the entire deep channel, which significantly enhanced the radial heat transfer.

5. Conclusions

In this paper, the interrelationships between the velocity field, velocity gradient field, and temperature gradient field of the melt during the polymer extrusion process were investigated theoretically, and the polymeric field synergy principle was proposed. Compared with standard screw, the flow, mixing, and heat transfer performance of four unconventional screws were explored using finite element method, and field synergy analysis was conducted. The conclusions are as follows:

1) In comparison to the plunger advection-flow generated in the STD screw, the BM screw realized the separation of solids-bed and melt though the auxiliary thread; the pin screw revealed a distinct diversion by rows of arranged pins. The eccentric structure of the wavy screw caused a periodic variation in the radial channel depth, generating extensional flow in the variational cross section. The unique structural design of the Maddock element with alternating deep and shallow channels, induced a distinctive helical flow pattern. Besides, radial convection was weak among these screws except the Maddock element and the intersection of deep and shallow channels of wavy screw.
2) Compared to the STD screw, different flow patterns induced by the unconventional screw elements can increase the stretching deformation of polymer melt. Among them, the improvement is most pronounced with the Maddock element, indicating that the helical flow can cause radial flipping of the fluid, enhancing radial mass transfer. Simultaneously, it greatly promoted the synergistic action between the velocity field and velocity gradient field, thereby improving the efficiency of the mixing process.
3) Heat transfer analysis indicated that the helical flow induced by the Maddock element can promote the extension of the high-temperature region towards the inner wall of the barrel. Simultaneously, the change in the velocity direction caused by the helical flow improved the synergistic action between the velocity field and the temperature gradient field, significantly enhancing the efficiency of heat and mass transport, thereby increasing energy utilization.

The study validated the scientific validity of the polymer field synergy principle and elucidated the intrinsic mechanism of heat and mass transport during polymer extrusion, which provides a new theoretical guidance for enhancing the mixing process efficiency and energy utilization of polymer extrusion equipment.

Author contributions: Conceptualization, WP; methodology, WP and RJ; investigation, WP, SH and RJ; writing—original draft preparation, WP, SH and RJ; writing—review and editing, WP, WY, XZ and RJ; visualization, WP, SH, JZ and RJ; supervision, RJ; project administration, RJ; funding acquisition, RJ. All authors have read and agreed to the published version of the manuscript.

Funding: This work was supported by the National Natural Science Foundation of China (grant number 52206095); the Shandong Provincial Natural Science Foundation (grant number ZR2021QE232); and the Youth Innovation Project for Universities of Shandong Province (2023KJ102). We also thank Mohini Sain from the University of Toronto for his assistance in improving the English of this work.

Conflict of interest: The authors declare no conflict of interest.

Nomenclature:

ρ	density	kg/m^3
$\vec{v}$	fluid velocity vector	m/s
$\vec{\tau}$	stress tensor	Pa
P	pressure	Pa
g	gravitational acceleration	9.80 m/s^2
$\overrightarrow{\nabla v}$	velocity gradient vector	s^{-1}
t	time	s
α	interaction angle between velocity and velocity gradient	°
C_v	constant-volume specific heat capacity	J/(kg·K)
T	fluid temperature	K
$\vec{q}$	heat flux	W/m^2
$\overrightarrow{\nabla T}$	temperature gradient vector	K/m
K	heat transfer coefficient	W/(m^2·K)
β	interaction angle between velocity and temperature gradient	°
L_1	barrel length	mm
L_2	screw length	mm
D	screw diameter	mm
d	screw root diameter	mm
S	screw pitch	mm
u_i	i-velocity component in rectangular coordinate system	m/s
x_i	i-coordinate component in rectangular coordinate system	m
x_j	j-coordinate component in rectangular coordinate system	m
η	apparent viscosity	Pa·s
C_p	constant-pressure specific heat capacity	J/(kg·K)
φ	viscous dissipation term	-
η_0	zero shear viscosity	Pa·s
η_∞	viscosity at an infinite shear rate	Pa·s
λ	natural time	s
$\dot{\gamma}$	shear rate	s^{-1}
n	non-Newtonian index	-
T_α	reference temperature	K
k	thermal conductivity	W/(m·K)
f	coefficient of temperature sensibility	K^{-1}

References

1. Dong H, Liu Y, Zhao Z, et al. Carbon neutrality commitment for China: from vision to action. Sustainability Science. 2022; 17(5): 1741-1755. doi: 10.1007/s11625-022-01094-2
2. Dong H, Xue M, Xiao Y, et al. Do carbon emissions impact the health of residents? Considering China's industrialization and urbanization. Science of The Total Environment. 2021; 758: 143688. doi: 10.1016/j.scitotenv.2020.143688
3. Yu S, Xiang H, Zhou J, et al. Typical polymer fiber materials: An overview and outlook. Acta Polymerica Sinica. 2020; 51(1): 39-54. doi:10.11777/j.issn1000-3304.2020.19148

4. Li W, Liu Q, Zhang Y, et al. Biodegradable Materials and Green Processing for Green Electronics. Advanced Materials. 2020; 32(33). doi: 10.1002/adma.202001591
5. Abeykoon C, Kelly AL, Vera-Sorroche J, et al. Process efficiency in polymer extrusion: Correlation between the energy demand and melt thermal stability. Applied Energy. 2014; 135: 560-571. doi: 10.1016/j.apenergy.2014.08.086
6. Deng J, Li K, Harkin-Jones E, et al. Energy monitoring and quality control of a single screw extruder. Applied Energy. 2014; 113: 1775-1785. doi: 10.1016/j.apenergy.2013.08.084
7. Dray RF. How to compare barrier screws. Plastics Technology. 2002; 48(12): 46-49, 59.
8. Chen J, Dai P, Yao H, et al. Numerical analysis of mixing performance of mixing section in pin-barrel single-screw extruder. Journal of Polymer Engineering. 2011; 31(1): 53-62. doi: 10.1515/polyeng.2011.009
9. Liu T, Du Y, He X. Statistical research on the mixing properties of wave based screws by numerical simulations. International Polymer Processing. 2023; 38(2): 200-213. doi: 10.1515/ipp-2022-4253
10. Spalding MA, Sun X, Kodjie SL, et al. A maddock mixer design that mitigates gels in polyethylene resin film applications. Journal of Plastic Film & Sheeting. 2022; 39(2): 174-189. doi: 10.1177/87560879221124172
11. Formela K, Cysewska M, Haponiuk J. The influence of screw configuration and screw speed of co-rotating twin screw extruder on the properties of products obtained by thermomechanical reclaiming of ground tire rubber. Polimery. 2014; 59(02): 170-177. doi: 10.14314/polimery.2014.170
12. Jian R, Dai R, Sain M, et al. Ductile behavior and heat transfer efficiency in polymer extrusion by self-controlled “flipping melt-pancakes” with multi-fields synergy. International Journal of Heat and Mass Transfer. 2022; 186: 122517. doi: 10.1016/j.ijheatmasstransfer.2021.122517
13. Jian R, Dai R, Sain M, et al. A strategy of stretching melt to a thin layer: Self-controlled “stretching melt-pancakes” to enhance heat transfer and mixing during polymer extrusion. Applied Thermal Engineering. 2023; 224: 120090. doi: 10.1016/j.applthermaleng.2023.120090
14. Abeykoon C, Pérez P, Kelly AL. The effect of materials’ rheology on process energy consumption and melt thermal quality in polymer extrusion. Polymer Engineering & Science. 2020; 60(6): 1244-1265. doi: 10.1002/pen.25377
15. Jian R, Yang W, Xie P, et al. Enhancing a multi-field-synergy process for polymer composite plasticization: A novel design concept for screw to facilitate phase-to-phase thermal and molecular mobility. Applied Thermal Engineering. 2020; 164: 114448. doi: 10.1016/j.applthermaleng.2019.114448
16. Jian R, Shi Z, Liu H, et al. Enhancing Mixing and Thermal Management of Recycled Carbon Composite Systems by Torsion-Induced Phase-to-Phase Thermal and Molecular Mobility. Polymers. 2020; 12(4): 771. doi: 10.3390/polym12040771
17. Jian R, Xie P, Liu H, et al. Ductile forming of polymers by inducing torsional flow to enhance heat transfer and mixing. Journal of Materials Processing Technology. 2020; 283: 116715. doi: 10.1016/j.jmatprotec.2020.116715
18. Jian R, Yang W, Cheng L, et al. Numerical analysis of enhanced heat transfer by incorporating torsion elements in the homogenizing section of polymer plasticization with the field synergy principle. International Journal of Heat and Mass Transfer. 2017; 115: 946-953. doi: 10.1016/j.ijheatmasstransfer.2017.07.121
19. Dhakal P, Das SR, Poudyal H, et al. Numerical simulations of partially‐filled rubber mixing in a 2‐wing rotor‐equipped chamber. Journal of Applied Polymer Science. 2016; 134(2). doi: 10.1002/app.44250
20. Gaspar-Cunha A, Covas JA. The Plasticating Sequence in Barrier Extrusion Screws Part II: Experimental Assessment. Polymer-Plastics Technology and Engineering. 2014; 53(14): 1456-1466. doi: 10.1080/03602559.2014.909482
21. Zitzenbacher G, Karlbauer R, Thiel H. A New Calculation Model and Optimization Method for Maddock Mixers in Single Screw Plasticising Technology. International Polymer Processing. 2007; 22(1): 73-81. doi: 10.3139/217.0109
22. Dörner M, Marschik C, Schöppner V, et al. Development of an Analytical Model to Describe the Disperse Melting in Wave-Dispersion Screws. Polymers. 2020; 12(4): 946. doi: 10.3390/polym12040946